

METALLICITY GRADIENTS IN M31, M33, NGC 300 AND THE MILKY WAY USING ABUNDANCES OF DIFFERENT ELEMENTS

Miriam Peña¹ and Sheila N. Flores-Durán¹

RESUMEN

Estudiamos los gradientes de metalicidad de O, Ne y Ar, derivados de nebulosas planetarias (PNe), en comparación con los de regiones H II en las galaxias M 31, M 33, NGC 300 y la Vía Láctea. Radios galactocéntricos y abundancias fueron recopilados de la literatura, seleccionando con cuidado una muestra homogénea de objetos en cada galaxia. Los gradientes de las PNe son más planos que los de las regiones H II en todos los casos. El caso más extremo es el de M 31, donde las abundancias de las PNe no están relacionadas con la distancia galactocéntrica y los gradientes son consistentes con cero. Calculamos gradientes para PNe del Tipo I y no-Tipo I de Peimbert, encontrando que los gradientes del Tipo I son más empinados y más similares a los de las regiones H II, lo que indicaría que los gradientes de metalicidad se empinan con el tiempo. Alternativamente los gradientes planos de las viejas PNe indican que la migración radial juega un importante papel en las galaxias.

ABSTRACT

Metallicity gradients derived from planetary nebulae (PNe) using O, Ne, and Ar abundances are studied and compared to those from H II regions in the galaxies M 31, M 33, NGC 300 and the Milky Way. Galactocentric radii and chemical abundances were collected from the literature, carefully selecting a homogeneous sample for each galaxy. Metallicity gradients shown by PNe are flatter than those of H II regions in all cases. The extreme case is M 31 where PN abundances are not related to galactocentric distances and the gradients are consistent with **zero**. To analyze the evolution of gradients with time we build gradients for Peimbert Type I and non-Type I PNe finding that Type I PNe show steeper gradients than non-Type I PNe and more similar to the ones of H II regions indicating that the chemical gradients might steepen with time. Alternatively, the flat gradients for old PNe show that radial migration could have an important role in the evolution of galaxies.

Key Words: galaxies: spiral — galaxies: ISM: abundances — planetary nebulae: abundances — Galaxies: individual: M 31, M 33, NGC 300 — The Galaxy

1. INTRODUCTION

Metallicity gradients in disk galaxies, provided by the analysis of the chemistry of H II regions at different galactocentric distances, have been studied since long ago (Aller 1942; Searle 1971, and many others), as such an analysis gives information on the chemical history of the host galaxy. The history of star formation and the processes of accretion and mass loss in a galaxy can be determined by using chemical evolution models that reproduce the present chemical abundances of the interstellar medium (ISM) using the abundances of H II regions as constraint. See e.g., Carigi & Peimbert (2011).

It has been found that metallicity gradients obtained from H II regions and other indicators are always negative, that is, chemical abundances are lower at larger galactocentric distances. Many galaxies have been

¹Instituto de Astronomía, Universidad Nacional Autónoma de México, Apdo. Postal 70264, Ciudad de México, 04510, México.

analyzed showing the same result. Recently Sánchez et al. (2014) analyzed the O abundance in a large number of H II regions in more than 300 galaxies observed by the CALIFA survey, reporting that in many galaxies with H II regions detected beyond two disk effective radii, the slope presents a flattening at large distances and in some cases a drop or truncation of the O abundance occurs in the inner regions.

Since some time ago the abundances determined for PNe are being also used to analyze the chemical gradients in galaxies. Among the oldest studies of PNe in the Milky Way we find that by D’Odorico, Peimbert, & Sabbadin (1976) and Kaler (1980). As PNe are objects with ages between 1 and 10 Gyr, they provide information of the past ISM abundances, helping then in the determination of the evolution of the chemical abundances in a galaxy, and providing additional constraints for the chemical evolution models of a galaxy (Hernández-Martínez et al. 2011).

Oxygen is the most used element to determine the chemistry of H II regions because its abundance in these photoionized nebulae is well determined by just adding the ionic abundances of O^+ and O^{++} , whose lines are observed in the visual range of wavelengths. The determination of ionic abundances requires the determination of physical conditions in the plasma, in particular the electron temperature which can be derived also in the visual range by detecting the faint auroral lines $[OIII] \lambda 4363$ and $[NII] \lambda 5755$, in order to use the so called *direct-method* to determine abundances.

Gradients based on oxygen abundances have been also calculated from PN data although for the case of highly ionized objects a correction due to the presence of O^{+3} is required. However, it has been shown that O in PNe may be enriched (or depleted) due to stellar nucleosynthesis, particularly in low-metallicity environments (Peña, Stasińska, & Richer 2007; Flores-Durán, Peña, & Ruiz 2017) and also in Galactic PNe with carbon-rich dust (Delgado-Inglada et al. 2015). Therefore metallicity gradients derived from O abundances in PNe could be perturbed by stellar nucleosynthesis and thus this element could be not adequate to analyze the chemical gradients and the evolution of galaxies. Apparently Ne abundances are also modified by stellar nucleosynthesis in low-metallicity environments (Karakas 2010; Milingo et al. 2010; Flores-Durán, Peña, & Ruiz 2017). On the other hand, Ar and S abundances in PNe are not expected to be modified in such processes during the PN progenitor lifetime, although their abundance determinations have large uncertainties due to large uncertainties in the ionization correction factors when only one ion (Ar^{++} or S^+) is observed (Delgado-Inglada, Morisset, & Stasińska 2014). Especially S abundance presents several problems, like ‘the Sulphur anomaly’. See e.g., Henry et al. (2010).

Considering the above, in this work we propose to use Ar/H, together with O/H and Ne/H abundance ratios, to trace the PN metallicity gradients in the galaxies of the local universe M31, M33, NGC 300, and the Milky Way (MW). Gradients of PNe will be discussed in comparison with those of H II regions. In §2 we present the data used for the different galaxies. In §3 the abundance gradients are calculated for each galaxy. In §4 our results are presented and discussed, and our conclusions are indicated in §5.

2. DATA ACQUISITION

Data used in this work consist of abundances and galactocentric distances of PNe and H II regions of the spiral galaxies M31, M33, NGC 300, and the Milky Way. Most data were obtained from the literature trying to include only abundances calculated with the *direct-method* (electron temperature determined), in a homogeneous way by one group of authors. However in some cases data from different sources have been included in order to obtain a larger sample of objects for statistical studies, covering as much galactic radius as possible. This introduced some degree of inhomogeneity that has been minimized by adopting only objects with electron temperature determined and by using recent ionization correction factors. We have selected samples where O, Ne, and Ar abundances are available.

We intend to build gradients based only on data from genuine PNe and H II regions, therefore for all the galaxies, we carefully selected as genuine PNe those objects where $[OIII] \lambda 5007$ intensity, relative to $H\beta$ is larger than 3, because a lower value could correspond to a compact H II region and not to a bona-fide PN. This criterium has been used for instance by Ciardullo et al. (2002) to select PNe to build the PNLF in external galaxies. On the other hand, H II regions showing $[OIII] \lambda 5007$ intensity larger than 3 times $H\beta$ were eliminated from the sample because these objects could correspond to nebulae around WR stars or SN remnants, whose abundances can be contaminated by the processes in the central stars and would not correspond to abundances of authentic pre-star nebulae.

TABLE 1
CHARACTERISTICS OF GALAXIES

Name	Hubble Type	Mass M_{\odot}	Dist (kpc)	O/H ^(a)	R_{25} (kpc)	ref. for R_{25} ^(b)
M 31	SA(s)b	1.5E12	785	8.8	20.6	D14
MW	SBbc	8.0E11	—	8.8	11.5	S-M18
M 33	SA(s)cd	5.0E10	849	8.5	9.0	M07
NGC 300	SA(s)d	3.5E10	1880	8.6	5.3	B09

^(a) O/H is the abundance at $R=0$, $12+\log O/H$, from H II regions.

^(b) D14: Draine et al. (2014), M07: Magrini, Corbelli, & Galli (2007)

B09: Bresolin et al. (2009), S-M18: Sánchez-Menguiano et al. (2018)

In Table 1 we present several characteristics of the studied galaxies such as their Hubble type, mass, distance to the Milky Way and the optical radius R_{25} (the 25 mag arcsec⁻² isophotal radius).

2.1. M 31

The well known M 31 is the most massive spiral galaxy in the Local Group. It is at a distance of 785 kpc from the Milky Way (McConnachie et al. 2005).

Chemical gradients calculated from the abundances of H II regions have been studied by several authors, most of the times based on abundances derived by using *strong-line* methods because due to the high metallicity in this galaxy, the auroral lines indicative of electron temperature, such as [O III] λ 4363 and [N II] λ 5755, are faint and difficult to detect. The biggest sample analyzed in this way is the one by Sanders et al. (2012), which included 192 H II regions. They reported an O abundance gradient of about -0.0195 ± 0.0055 dex kpc⁻¹, but found that the slope depends on the choice of the *strong-line* method used.

Zurita & Bresolin (2012) obtained abundances based on the *direct-method* for 31 H II regions concentrated at two galactocentric distances of 3.9 and 16.1 kpc. These authors discussed the O/H abundance gradient finding a robust negative slope of $\Delta O/H / \Delta R = -0.023$ dex kpc⁻¹ based on both, the *direct-method* and the *strong-line* method. This value is similar to the values reported by other authors, based on *strong-line* methods (Zaritsky, Kennicutt, & Huchra 1994; Sanders et al. 2012).

Interestingly, Zurita & Bresolin (2012) found that O abundances, determined with the *direct-method* in their H II regions, are lower, by about 0.3 dex, than the values determined with the *strong-line* methods and the values derived for supergiant stars, at any galactocentric distance. The authors attribute this discrepancy to a bias in their sample which would be not representative of the mean H II region population (because only high-temperature regions, and thus of low metallicity, could be detected in their search), and to the probable depletion of O in dust grains. Abundance data for H II regions, used in this work, are taken from Zurita & Bresolin (2012).

Data for PNe were collected from the articles by Kwitter et al. (2012); Sanders et al. (2012); Balick et al. (2013); and Fang et al. (2013, 2015). The use of data from different authors can introduce undesirable inhomogeneities, therefore, in order to analyze chemical abundances on a more homogeneous system, physical conditions and ionic abundances of PNe were recalculated by us from the extinction-corrected line intensities published by the cited authors. The IRAF 2.16 five level nebular modelling package "stsdas.analysis.nebular", with the tasks *temden* and *ionic*, were employed to determine physical conditions and ionic abundances. For all the sample the [O III] temperature was derived and occasionally the [N II] temperature was available, but all the ionic abundances were calculated with the [O III] temperature (one-temperature zone model). Total abundances were derived from the ionic abundances by using the ionization correction factors (ICFs) by Delgado-Inglada, Morisset, & Stasińska (2014) to correct for the not seen ions. The results, although not too different from the ones published by the cited authors, are now in a homogeneous system.

The PN distribution in this galaxy extends up to $R/R_{25} \sim 5$ ($R \geq 100$ kpc) while data for the H II regions cover only up to $R/R_{25} \sim 1$ ($R \sim 20$ kpc).

The galactocentric distances used in the diagrams for the gradients were collected from the same references used for the abundance ratios.

2.2. M 33

M 33 is the third spiral galaxy in the Local Group. Its Hubble type is very late, SA(s)cd, and its mass is much lower than the masses of the Milky Way and M 31, by factors of 16 and 30 respectively. It is located at 849 kpc from the Milky Way and appears almost face-on. The central metallicity in M 33 as given by H II regions, $12+\log \text{O}/\text{H} = 8.5$, is lower than in the bigger spirals, and it is even lower than in NGC 300 (see Table 2).

Gradients from PN abundances are found in Magrini, Stanghellini, & Villaver (2009) and Bresolin et al. (2010) who found that the slopes are equal to the ones of H II regions or flatter, respectively.

For this galaxy, PN data were collected from Bresolin et al. (2010) and Magrini et al. (2010), and H II region data are from Magrini et al. (2010). The distributions of H II regions and PNe extend up to $R/R_{25} \simeq 1$ ($R \sim 9$ kpc). As said in the Introduction, in the sample of PNe we excluded those objects showing $[\text{OIII}]\lambda 5007/\text{H}\beta$ intensity ratio lower than 3 and consistently, for the H II regions we excluded the objects showing this ratio larger than 3. This is to avoid contamination by compact H II regions in the PN sample and to avoid contamination by supernova remnants, W-R nebulae and other highly excited objects in the H II region sample. Our diagrams then contain only genuine PNe and H II regions.

The galactocentric distances employed to build the gradient diagrams were calculated by us, according to the procedure described by Cioni (2009).

2.3. NGC 300

The almost face-on spiral NGC 300 is the less massive galaxy of the all sample studied here and the only one out of the Local Group. Also it is the latest in terms of the Hubble type, SA(s)d. It is similar to M 33 in several aspects. Analysis of the H II regions have been made by several authors. Bresolin et al. (2009) were the first to determine the oxygen abundance gradient based on *direct-method* abundance determinations, they found $\Delta\text{O}/\Delta R = -0.077$ dex kpc^{-1} with a central abundance of $12+\log \text{O}/\text{H} \simeq 8.57$.

Stasińska et al. (2013) analyzed the chemical gradients provided by H II region and PN abundances finding that gradients for PNe appear flatter than those of H II regions.

In this work we have re-analyzed the PN data presented by Stasińska et al. (2013), to make a comparison of the case of NGC 300 with the other galaxies of the sample. Abundances presented by Stasińska et al. (2013) were derived by adopting the ICFs proposed by Kingsburgh & Barlow (1994), and in this work we have used the more recent ICFs presented by Delgado-Inglada, Morisset, & Stasińska (2014). With these new ICFs we found that our O/H values are equal to the Stasińska et al. (2013) ones with differences lower than 0.03 dex, Ne/H values show differences, in average, lower than 0.05 dex, while our Ar/H values are different from those by Stasińska et al. (2013) by 0.07 dex in average. Data for H II regions are from Bresolin et al. (2009).

In this galaxy PNe and H II regions have been found up to $R/R_{25} \simeq 1$ ($R \sim 5$ kpc). Galactocentric distances were collected from the same authors as in the abundances.

2.4. Milky Way

Metallicity gradients have been widely studied in the MW by means of H II regions, PNe, Cepheid stars, stellar clusters and other objects. See e.g., Deharveng et al. (2000); Maciel, Costa, & Ushida (2003); Henry et al. (2010); Stanghellini & Haywood (2018, 2010); Esteban et al. (2017); the compilation by Mollá et al. (2019), etc. The reported results for PNe have been contradictory. It has been claimed that the PN gradients coincide with those of H II regions or that the PN gradients are shallower, that gradients have flattened (or steepened) with time, or that the gradient changes of slope at certain distance from the galactic center. One of the main problem in these determinations is the large uncertainties in the distances to PNe.

Determining the distance to galactic PNe is a difficult task. The trigonometric parallax method is available only for a handful of nearby objects. Even the parallaxes measured by GAIA are limited to distances of a few kpc around the solar system, and in GAIA Data Release 2 less than a hundred PNe have confident measured parallaxes (Kimeswenger & Barriá 2018). Therefore, the distances for a large sample of PNe are based on model-dependent statistical methods which in occasions lead to different results. To the present the most used distance scales are those proposed by Stanghellini & Haywood (2010), hereafter S10, and by Frew, Parker, & Bojičić

(2016), hereafter F16. The latter authors established a robust optical statistical distance indicator, the $H\alpha$ surface brightness vs. radius ($S_{H\alpha}$ -r) indicator, where the intrinsic radius is calculated by using the angular size, the integrated $H\alpha$ flux, and the reddening to the PNe. This radius, combined with the angular size, yields directly the distance. On the other hand, S10 determine statistical distances based on apparent diameters and 5 GHz fluxes of PNe. A comparison of both distance scales are presented further below.

In this work we used PN chemical abundances reported by Henry, Kwitter, & Balick (2004), Milingo et al. (2010), and Henry et al. (2010). These authors belong to the same group therefore all physical conditions were calculated with the same systematical method and total chemical abundances were obtained using the ICFs described in Kwitter & Henry (2001). The Galactic sample consists of 156 PNe covering galactocentric distances in the range $0.21 \text{ kpc} \leq R \leq 22.73 \text{ kpc}$ ($0.02 \leq R/R_{25} \leq 1.97$). More than 40 of these PNe lie at distances larger than the solar galactocentric distance and are crucial for the gradient determination.

In the case of H II regions, oxygen abundances were taken from Esteban et al. (2017), while neon and argon abundances were collected from García-Rojas et al. (2004), García-Rojas et al. (2005), García-Rojas et al. (2006), García-Rojas et al. (2007), Esteban et al. (2004), Esteban et al. (2013), and Fernández-Martín et al. (2017). As said above, the use of data processed by different authors can introduce some inhomogeneities and uncertainties in the Ne and Ar gradients of H II regions, that should be considered carefully.

In Fig. 6 we present the comparison of the metallicity gradients of oxygen, argon and neon for the Galactic H II regions and the PN sample. This figure will be discussed in detail in §3.4, here we want to show that for the case of PNe we are using the distances by F16 and S10 for a comparison. As seen in this figure the oxygen, neon, and argon abundances present a very large dispersion at all galactocentric distances, but the linear regressions for PNe are similar for both distance indicators. Therefore in the following F16 distances will be used as an independent way to compare with other works.

3. ABUNDANCE GRADIENTS

Abundance gradients of the different elements for the different galaxies were calculated by fitting a straight line to the abundances versus the fractional galactocentric distance R/R_{25} and also versus the distance R (kpc). For each elemental abundance we computed one fit for PNe and one for H II regions. Gradients are shown in the respective figures. In Table 2 a compendium of the abundance gradients versus galactocentric distance R (kpc) is listed. For each fit the table gives the values at the intercept, X_0 , and the slope, calculated in the equation:

$$Y = X_0 + \Delta X/\Delta R \times R \text{ (kpc)}.$$

Errors have been calculated at 1 sigma. The errors in the gradients of Ne and Ar are much larger than in O, due to the large dispersion in the abundances at any galactocentric distance and due to the uncertainties in the abundance determination because large ICFs are used for these elements.

3.1. *M31*

In Fig. 1 the radial gradients for O/H, Ne/H and Ar/H, for PN and H II region abundances are presented vs. R/R_{25} . The gradients vs. R (kpc) are presented in Table 2.

A linear fit to the gradients is included in each case. The abundances of elements in PNe present a large dispersion at any given galactocentric distance, but in particular in the central zone. It is worth to notice that there are some PNe in the central region with very low O/H abundance, which do not have Ne/H or Ar/H abundance determinations. H II regions also present a large dispersion in the elemental abundances at any galactocentric distance (Zurita & Bresolin 2012; Sanders et al. 2012).

For the case of O in H II regions, it is obtained:

$$12+\log(\text{O}/\text{H}) = (8.76 \pm 0.10) - (0.679 \pm 0.153) R/R_{25}$$

or equivalently

$$12+\log(\text{O}/\text{H}) = (8.76 \pm 0.10) - (0.030 \pm 0.007) R \text{ (kpc)}.$$

The O gradient found is equal within uncertainties to one derived by Zurita & Bresolin (2012).

For Ne, we find $12+\log(\text{Ne}/\text{H}) = (7.99 \pm 0.23) - (0.036 \pm 0.016) R$ (kpc), and for Ar, we find $12+\log(\text{Ar}/\text{H}) = (6.38 \pm 0.018) - (0.021 \pm 0.013) R$ (kpc)

In all the cases, the errors correspond to 1 sigma

PN abundances seem not related to the galactocentric distance and the PN gradients are really flat, showing slopes of -0.001 ± 0.001 dex kpc^{-1} for O, -0.002 ± 0.001 dex kpc^{-1} for Ne, and -0.002 ± 0.001 dex kpc^{-1} for Ar, which considering the errors, are consistent with 0. This indicates that at large galactocentric distances PNe present in average the same O/H abundances that in the central zones and the same is true for Ar and Ne.

The O/H value at the intercept for H II regions, $12+\log \text{O}/\text{H} = 8.76 \pm 0.10$, seems slightly larger than the value for PNe, $12+\log \text{O}/\text{H} = 8.46 \pm 0.03$, while Ne/H and Ar/H central values are similar for H II regions and PNe, within uncertainties. However, due to the negative gradients for H II regions, at large distances ($R \leq R_{25}$), O/H, Ne/H and Ar/H abundances in PNe are always larger than abundances in H II regions.

The larger value of O at the intercept for H II regions seems an artifact due to the limited sample by Zurita & Bresolin (2012) which moreover present large uncertainties. In addition, there are a large number of PNe with low O abundances in the central zone, with no Ne and Ar measurement, that could be contributing to the low O/H central value for PNe. In this zone a very large dispersion is observed.

In the central zone the value at $R=0$ of $\log \text{Ne}/\text{O} = -0.77$ in H II regions is about solar and discards the possibility indicated by Zurita & Bresolin (2012) of a large O depletion in dust grains. On the other hand, Ne in H II regions is similar to Ne in PNe in the central zone. Relative to Ar, $\log \text{Ar}/\text{O} (\text{H II}) = -2.38$ and $\log \text{Ar}/\text{O} (\text{PNe}) = -2.24$ which correspond well with the solar or Orion values.

In Fig. 2 we show the abundance gradients for PNe separated in Peimbert types. Peimbert (1978) called Type I those PNe with N/O abundance ratio larger than 0.5 and He/H abundance ratio larger than 0.14. This group includes the PNe with central stars with initial mass larger than about $3.0 M_{\odot}$ and therefore they are the youngest objects among PNe. They have enriched their nitrogen abundances in nucleosynthesis processes such as CNO and hot-bottom-burning (HBB) and the newly formed N has been transported to the surface in different dredge-up events. In the Galaxy, Type I PNe belong to the thin disk and their ages are about 1 Gyr. Non-Type I PNe include the Peimbert Types II and III PNe which are classified based on their radial velocity, smaller or larger than 60 km s^{-1} , and are located in the thick disk. They correspond to older objects with initial masses lower than $2 M_{\odot}$, where no such a large N-enrichment is appreciated. Their ages are between 2 to 8 Gyr.

Thus our Fig. 2 represents an effort to determine the behavior of the abundance gradient with time. It is evident that although the gradients are very flat and the uncertainties are large, Type I PNe show slightly steeper gradients for the three elements: O, Ne and Ar. Additionally, Type I PNe seem to be O-poorer than non-Type I, possible showing the effect of CNO and HBB processes which operates in these massive stars. This phenomenon will be discuss with more detail in §4.1.

It should be mentioned here that the value for N/O abundance ratio, to define a Peimbert Type I PN is slightly dependent on the metallicity. The N/O ratio defined by Peimbert (1978) applies to the metallicities of the Milky Way and M31, and should be slightly lower for M33 and NGC 300, but the difference is not important for this work and the results are not much affected.

We will discuss the results for M31 in sections ahead, together with the results for the other galaxies.

3.2. M33

Metallicity gradients for H II regions and PNe in M33 are presented in Figs. 3 and 4. In the latter one, PNe are separated in Peimbert Type I and non-Type I objects. Differently to what happens in M31, in this galaxy O, Ne and Ar abundances of PNe and H II regions are similar within uncertainties, at any galactocentric distance.

For PNe the straight-line fit of the gradients gives $12+\log \text{O}/\text{H} = (8.34 \pm 0.07) - (0.038 \pm 0.016) R$ (kpc) and for H II regions, $12+\log \text{O}/\text{H} = (8.48 \pm 0.03) - (0.047 \pm 0.008) R$ (kpc). That is, the slope for PNe seems shallower than the slope in H II regions, by about 30% for O and larger factors for Ne and Ar, but the uncertainties are large making these results not conclusive. However we consider indicative that PN gradients are shallower.

In Fig. 4, the gradients of PNe with different Peimbert Types are shown. There are only a few Type I PNe in the sample (about 20%) and the uncertainties are very large, however the central values can be considered equal within errors, for both PN types. Despite the uncertainties, slightly steeper gradients are apparent for Type I PNe, while the gradients for non-Type I PNe are flatter. The slopes shown by Type I PNe are more similar to the ones presented by H II regions. The huge uncertainties in these results make them not conclusive,

but only indicative. We consider them confident because M33 would be showing similar results to M31 and NGC 300.

3.3. NGC 300

PN data in this galaxy were analyzed by Stasińska et al. (2013) where O, Ne, S and Ar abundance gradients were presented. These authors found that the formal O/H, Ne/H and Ar/H abundance slopes for PNe are shallower than those of H II regions and attributed this to a steepening of the metallicity gradients during the last Gyr. The O/H central value in PNe is smaller by 0.15 dex than the central value of H II regions. Ne/H and Ar/H on the other hand present the same central abundances in PNe and H II regions, and almost flat gradients, although affected by large dispersion at any galactocentric distance. According to Stasińska et al. (2013), due to the difference in the O/H value at R=0, O abundances in PNe could have been affected by nucleosynthesis of their central stars.

Our analysis of these data, calculated with the ICFs by Delgado-Inglada, Morisset, & Stasińska (2014) shows similar results that are presented in Fig. 5. O, Ne and Ar metallicity gradients for PNe in NGC 300 are flatter than the values of H II regions. Their $\Delta X/\Delta R$ values are about half the values found for H II regions, in very good agreement with the results by Stasińska et al. (2013). At the central zone, H II regions show $12+\log \text{O}/\text{H} = 8.57 \pm 0.03$, $\log \text{Ne}/\text{O} = -0.86 \pm 0.008$ and $\log \text{Ar}/\text{O} = -2.20 \pm 0.07$, these abundance ratios are similar to solar or Orion values, while PNe present values $12+\log \text{O}/\text{H} = 8.37 \pm 0.03$, $\log \text{Ne}/\text{O} = -0.73 \pm 0.06$, and $\log \text{Ar}/\text{O} = -2.06 \pm 0.05$, ratios also similar to the solar and Orion values but showing an apparent O decrease by 0.2 dex, relative to the O in H II regions, as it was already indicated by Stasińska et al. (2013). This will be discussed in §4. The central values of Ne/H and Ar/H are similar for PNe and H II regions.

In this case, an analysis discriminating between the Peimbert Type PNe is not possible, because there are very few Type I PNe in the sample.

3.4. The Milky Way

As said above metallicity gradients have been widely studied in the MW by means of many kind of objects. See references in §2.4.

Henry et al. (2010), using distances by Cahn, Kaler, & Stanghellini (1992) derived an O gradient for PNe of $-0.058 \pm 0.006 \text{ dex kpc}^{-1}$, which changes to $-0.042 \pm 0.004 \text{ dex kpc}^{-1}$ if the distances by Stanghellini, Shaw, & Villaver (2015) are used. Henry et al. (2010) suggested that the gradient steepens beyond a galactocentric distance of 10 kpc. In a recent work, Stanghellini & Haywood (2018), using distances given by S10, reported that out to $R/R_{25} \simeq 2.4$ ($R \sim 28 \text{ kpc}$) the radial gradient of oxygen for PNe is shallow, with slope $\sim -0.02 \text{ dex kpc}^{-1}$ and a central abundance of $12+\log(\text{O}/\text{H}) \simeq 8.68$. These authors suggest that the gradient changes with R in the sense that the significant slope is limited to R between 10 and 13.5 kpc and outside this range the gradient is almost flat.

We analyzed the gradients derived from the data for PNe and H II regions mentioned in §2.4. PN abundances were calculated by us in a homogeneous way. The results are presented in Figs. 6 and 7. In the latter figure the data have been binned in distance taking bins of 1 kpc, for clarity. The distances by F16 are used for PNe.

Clearly, PN gradients are flatter than those of H II regions. $\Delta X/\Delta R$ is about twice larger for H II regions (see Fig. 7 and Table 2). The binning of data with distances have introduced an artifact in Fig. 7 in the sense that O and Ne abundances for PNe seem larger than the values for H II regions, at R=0. But this does not occur in Fig. 6 where the original data, not binned, were used. In these graphs it is observed that the O and Ne values at the central zones coincide for PNe and H II regions, within uncertainties, while Ar/H abundance is lower in PNe by 0.7 dex. However due to the shallower gradients for PNe, at galactocentric distances larger than a few kpc, the average abundances in PNe are larger than in H II regions, similarly to what happens in M31 and NGC 300. By the way, this can explain part of the results by Rodríguez & Delgado-Inglada (2011) who found that in the solar vicinity, PNe appear richer than H II regions.

The gradients derived for PNe of different Peimbert types are shown in Fig. 8. In this case, gradients of Type I and non-Type I PNe are equal within uncertainties. A possible change in the slope, at $R \sim 14 \text{ kpc}$, is appreciated that will be discussed in the next section.

We used the known GAIA distances of PNe to analyze the gradient for PNe. Using the same set of abundances of the MW, we searched for those PNe that have calculated parallaxes on GAIA Data Release 2

(GAIA DR2). We did not take into account those objects with negative parallax and error in parallax (dp/p) bigger than 0.4. We found 22 PNe meeting these requirements. No gradient is found in this interval for the three analyzed elements, because GAIA galactocentric distances are limited from 6 to 10 kpc, and this interval is too short to show any gradient, due to the large dispersion in abundances.

4. RESULTS AND DISCUSSION

The radial gradients of the elements O, Ne and Ar are analyzed for homogeneous samples of PNe and H II regions in four disk galaxies of different Hubble type, different masses and different metallicities, M 31, M 33, NGC 300 and the Milky Way. A compendium of our results, with all the linear fits and slopes $\Delta X/\Delta R$ in dex kpc^{-1} , is presented in Table 2. In the following we discuss the results.

4.1. M 31

Our work extends the PN sample, including objects from 2 kpc up to a distance larger than 100 kpc ($0.2 - 5 R_{25}$). In this interval the abundance gradients for PNe are flat, consistent with a slope of zero. The average abundances of PNe are the same at all galactocentric distances, showing a very large dispersion.

On the other hand the gradients for H II regions are always negative, with values -0.030 ± 0.010 dex kpc^{-1} for O, -0.036 ± 0.016 dex kpc^{-1} for Ne and -0.021 ± 0.013 dex kpc^{-1} for Ar. These slopes are much shallower than the slopes in the other three galaxies. The very flat gradients found in M 31 could indicate, according to Sánchez et al. (2014), that M 31 has been perturbed by interactions or merging. It is clear that these phenomena have had an important role in the formation and growth of M 31, a galaxy that shows numerous stellar substructures in its outskirts (McConnachie et al. 2009, and references therein).

At the central position PNe appear to have an average O/H abundance slightly lower than the average in H II regions, but similar Ne/H and Ar/H abundances. This could be due to the presence of several PNe with very low O abundance (and not known Ne and Ar) in the central region, as it was explained in §3.1

The same as it is found in our work, Sanders et al. (2012) and Magrini et al. (2016) reported that the O/H gradient from PN abundances is flat in M 31. Sanders et al. (2012) in particular, from the analysis of O abundances in 52 PNe, derived with the *direct-method*, located at galactocentric distance from 5 to 25 kpc (0.2 to $1.2 R_{25}$), mentioned that there is no relation between PN abundances and their galactocentric distances. This same PN sample was re-analyzed by Magrini et al. (2016) who reported that radial migration plays an important role in PNe of M 31, which possibly explains the extreme flatness of PNe gradients, since PNe may have migrated far from their place of origin.

When the sample is divided in Peimbert Type I PNe (young objects) and non-Type I PNe (older objects), it is found that the young objects show a steeper gradient, although still very flat (Fig. 2). Due to their youth (ages lower than about 1 Gyr), Type I PNe have had less time to migrate from their birth places, then they might be showing the gradient at about 1 Gyr ago, but considering that these gradients are very flat compared to the ones of H II regions, migration should have had an important role for these young PNe too.

It is important to mention that the results found for M 31 corroborate models of galactic chemical evolution, which besides including the star formation rate, gas infall rate across the disk, inflows and outflows of gas, stellar evolution and yields, among other processes, also include radial redistribution of stars (stellar migration). Models by Ruiz-Lara et al. (2017) predict that radial redistribution and accretion increase the metallicity dispersion, and flatten the age and metallicity profiles of galaxies; the greater the efficiency of the redistribution, the larger the flattening effect and, as a consequence, steeper metallicity gradient should be expected at birth of the objects. Being Type I PNe closer to their birth places, they show steeper gradients.

Peimbert Type I PNe present slightly lower O abundances than non-Type I's, while Ne and Ar abundances are similar. This can be due to nucleosynthesis because CNO and HBB processes are expected to occur in these more massive central stars modifying their initial O abundance. Such an O decrease is predicted by recent sophisticated evolutionary stellar models for low-intermediate mass stars of the MW, computed at different metallicities, by Ventura et al. (2017). Using the sequence of models with $z \sim 0.014$ (solar metallicity) it is found that stars with masses larger than $3 M_{\odot}$ diminish their O/H abundance by up to 0.2 dex at the end of their evolution, while stars of lower masses do not modify their original O/H. This is the effect we are finding in the comparison of Type I and non-Type I PNe in M 31.

4.2. M33

In the case of M33, a late Hubble-type galaxy, the results are presented in Figs. 3 and 4. In this case O, Ne and Ar in PNe show similar central values to the values of H II regions therefore there is not important enrichment of the ISM since the time of formation of these PNe. Similarly, the O abundance gradients of PNe and H II regions are equal, within uncertainties, but the Ne and Ar abundance slopes in PNe seem significantly flatter, although the large dispersion and large uncertainties make these results doubtful.

Due to the similarity of metallicity gradients and the large dispersion, Magrini, Stanghellini, & Villaver (2009) claimed that gradients are equal for PNe and H II regions. In a recent paper, Magrini et al. (2016) analyzed the possible effects of radial migration in M33 and concluded that it is not important. Also Bresolin et al. (2010) declared that PNe and H II regions have equal gradients within uncertainties, but an analysis of their Table 8 shows that the slopes for PNe are systematically flatter than the slopes of H II regions, even when the uncertainties are large.

It is interesting to notice that PNe in M33 do not show O reduction compared to H II regions, as occurs in NGC 300 (see next section), despite the similar low metallicity in both galaxies. It seems that the initial masses of the central stars in this galaxy are not as large as in NGC 300, thus they are not affected by nucleosynthesis in the same way as in NGC 300. According to Ventura et al. (2016) models, the initial masses should have been not much larger than $2 M_{\odot}$.

Although the uncertainties are huge due to the low number of objects, Type I PNe in M33 seem to present slopes steeper than non-Type I PNe, and more similar to the ones of H II regions. Again these results are very uncertain, but we consider them indicative of the similar phenomenon occurring in M31.

4.3. NGC 300

For NGC 300, the latest Hubble-type galaxy, with metallicity similar to M33, the abundance gradients of PNe are about twice smaller than the gradients of H II regions (see Fig. 5). The gradients presented by H II regions are the largest ($\Delta O / \Delta R = -0.077 \pm 0.008 \text{ dex kpc}^{-1}$) in the whole galaxy sample.

The average O/H central abundance of PNe is lower than the value in H II regions by 0.2 dex, while Ne and Ar have the same central values. Such an O decrease, which does not occur in Ne and Ar, could be the result of stellar nucleosynthesis and dredge-up events. Stellar evolution models performed by Ventura et al. (2016) for PNe in the SMC (which has a metallicity similar to the NGC 300 one) predict a decreasing of the initial O occurring in stars with masses larger than $3 M_{\odot}$, due to HBB, simultaneously a large N-enrichment occurs. Such N-enrichment is observed in the PNe of NGC 300 (Stasińska et al. 2013). Therefore we conclude that the central stars of PNe analyzed in this galaxy had in general large initial masses and are younger than 1–2 Gyr. This is certainly due to a bias in the sample because only the brightest objects were observed at the NGC 300 distance (Peña et al. 2012).

The central values of Ne/H and Ar/H are similar for PNe and H II regions. Once again this indicates that PNe are young objects which had initial abundances similar to the present ISM.

An interesting fact is that at R/R_{25} larger than 0.6, Ar/H abundances of PNe are definitely larger than the values of H II regions, independent of the large dispersion. This is also found for Ne, but less marked. Since Ar it is not expected to have been modified by stellar nucleosynthesis of central stars, this is indicating that radial migration should have been important in PNe (despite their youth) and that PNe have changed their initial galactocentric distances, being churned in the galaxy, although not at the level of migration found in M31.

4.4. The Milky Way

The results for the MW are presented in Figs. 6 and 7. The latter figure shows PNe data with a bin of 1 kpc in distance. The PN sample covers a galactocentric distance interval $0.21 \text{ kpc} \leq R \leq 22.73 \text{ kpc}$ ($0.02 \leq R/R_{25} \leq 1.97$). The gradient obtained for O in PNe is $-0.024 \text{ dex kpc}^{-1}$, similar to the ones derived for Ne and Ar. As occurs in M31, and NGC 300, PN gradients are flatter, by about a factor of 2, than the gradients of H II regions.

The gradients for Type I and non-Type I PNe are shown in Fig. 8. In this figure the slopes of both kind of nebulae seem indistinguishable. Our result is different from what it was reported by Stanghellini & Haywood (2010) and Stanghellini & Haywood (2018) for their young and old PN samples, using the distances by S10.

They claim that young PNe definitely present a steeper gradient of $-0.027 \text{ dex kpc}^{-1}$ versus $-0.015 \text{ dex kpc}^{-1}$ for old PNe. We are not sure if our different result is due to the different PN samples (a much larger sample from the literature, not homogenized, was used by Stanghellini & Haywood (2018)) or the different distance scale used. In any case we coincide with them in that PN gradients are flatter than those of H II regions, therefore it appears that PNe have moved from their birth places due to radial migration and are showing flatter gradients. Alternatively it is possible that the abundance gradients were flatter several Gyr ago.

Although a linear fit to these gradients produces acceptable results, it should be noticed that at distances larger than about 14 kpc, the observed abundances (in particular O/H and Ar/H) decrease to a value below the linear fit and continue flat outwards, marking a step. Unfortunately in our sample there are few PNe out of these distances and this result is not conclusive. The same step at a distance $R \sim 13.5 \text{ kpc}$, was reported by Stanghellini & Haywood (2018) from the same sample of outer PNe. Following Halle et al. (2015) they attributed this behavior to the effect of the galactic bar whose outer Lindblad resonance would be located at about this distance according to N-body simulations for the galaxy. It is crucial to observe a larger number of PNe in the outskirts of the Galaxy to verify this behavior.

It is interesting to compare the gradients of H II regions ($-0.040 \text{ dex kpc}^{-1}$) and PNe ($-0.024 \text{ dex kpc}^{-1}$) with others provided by well measured indicators of different ages. Mollá et al. (2019) have prepared a compilation of gradients for different objects of different ages, computed by different authors, in order to compare them with results from their chemical evolution models. From this compilation we select the gradients calculated by Mollá et al. for Cepheid stars which are young objects with ages of about 0.1 Gyr, showing an O/H gradient of $-0.049 \text{ dex kpc}^{-1}$, and open clusters (OC) which span ages from 2 to more than 8 Gyr. The O/H gradient for OC with ages younger than 2 Gyr is $-0.030 \text{ dex kpc}^{-1}$, and for ages between 2 and more than 8 Gyr, the slope is $-0.027 \text{ dex kpc}^{-1}$. It is clear that the gradient of H II regions and Cepheid stars are equal within uncertainties indicating that in the Galaxy the chemical gradients have not changed significantly in at least the last 0.1 Gyr, while gradients of PNe (Type I's and non-Type I's) are equal to that of OC with ages older than 2 Gyr. Therefore for objects of 2–8 Gyr the gradient is flatter ($-0.027 \text{ dex kpc}^{-1}$) than those of Cepheids and H II regions (-0.049 and $-0.040 \text{ dex kpc}^{-1}$). PNe and OC certainly could have been affected by migration, but not in an as extreme way as in M31. Alternatively, PN and OC gradients could represent the true gradients at several Gyr ago.

In Mollá et al. (2019) it is discussed the possible effects of migration in the MW. By analyzing models by different authors, their conclusion is that radial migration seems to be not important for stars younger than 4 Gyr. Only for objects older than 8 Gyr, radial migration may be important. Models by Mollá et al. of time evolution of chemical gradients in the Milky Way (without considering migration, bar or spiral arms) predict a very smooth evolution of the radial gradient within the optical disk. Some model show a steepening of the gradient, from -0.02 to $-0.04 \text{ dex kpc}^{-1}$ from time equal to 10 Gyr until the present. Therefore the gradients presented by PNe and OC could be the gradients at the time of formation of these objects, not affected by migration.

5. CONCLUSIONS

From the analysis of abundance gradients of O, Ne, and Ar in PNe and H II regions in the four galaxies, it is found that in NGC 300 (a late Hubble-type spiral of low metallicity) and the Milky Way, the abundance gradients for PNe are flatter than those of H II regions, by factors of 2. This result is less conclusive in the case of M33, but also slightly flatter gradients are found for PNe than for H II regions.

M31 represents an extreme case where PN abundances are not related to the galactocentric distances and present the same values at any distance from the center up to more than a 100 kpc. Merging, interactions with other galaxies and important radial migration of PNe are causing this phenomenon in M31. It is worth to notice that considering the H II regions, M31 presents the shallower gradients of the four galaxies, which again is a possible consequence of merging and interactions.

In the four galaxies analyzed here, there is a large dispersion on abundances at any galactocentric distance which is larger for PNe than for H II regions. This possibly is caused by migration. PNe could have been churned in the galactic disk far from their birth places thus their abundances do not correspond to the place where they presently are. In trying to understand this it is important to analyze the abundances of elements that have been not modified by stellar nucleosynthesis, like Ar, as O and Ne can be modified depending on the

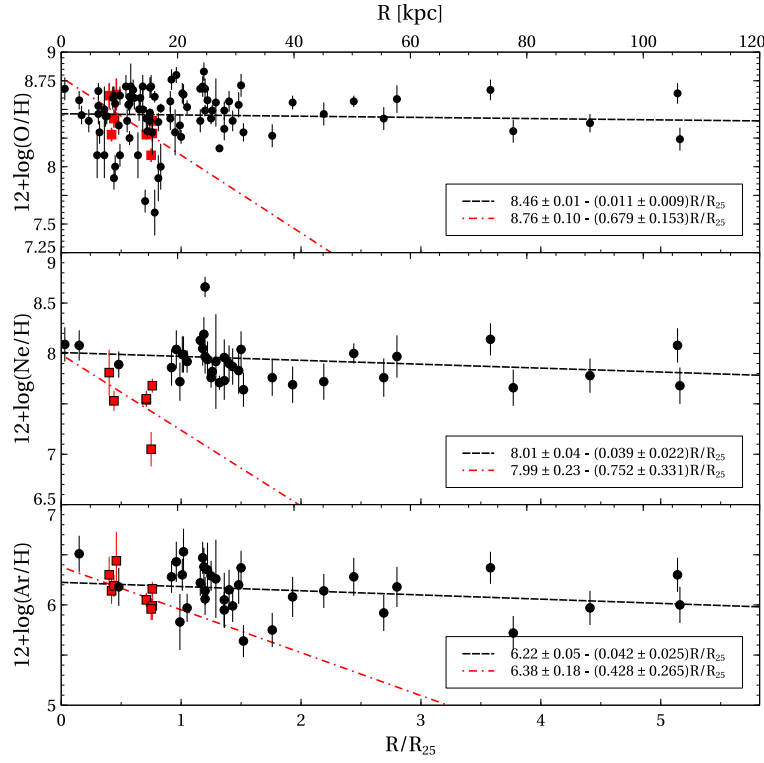


Fig. 1. Radial metallicity gradients of O (top), Ne (center) and Ar (bottom) for M31, are presented. Black circles represent PNe and red squares, H II regions. Black dashed lines correspond to the linear fit for PN data and dashed-dotted red lines correspond to the linear fits for H II regions respectively.

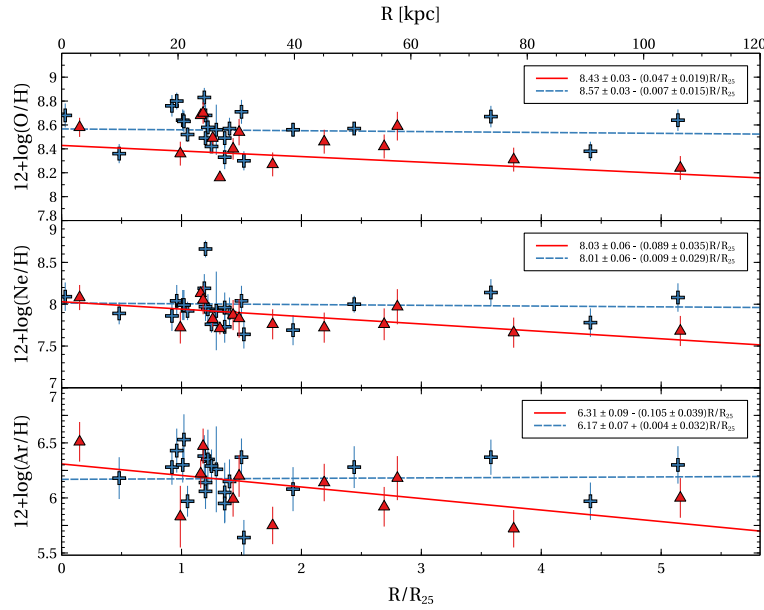


Fig. 2. Radial metallicity gradients for different Peimbert Type PNe in M31. In red the data for Type I PNe are shown and in blue, the data for non-Type I PNe.

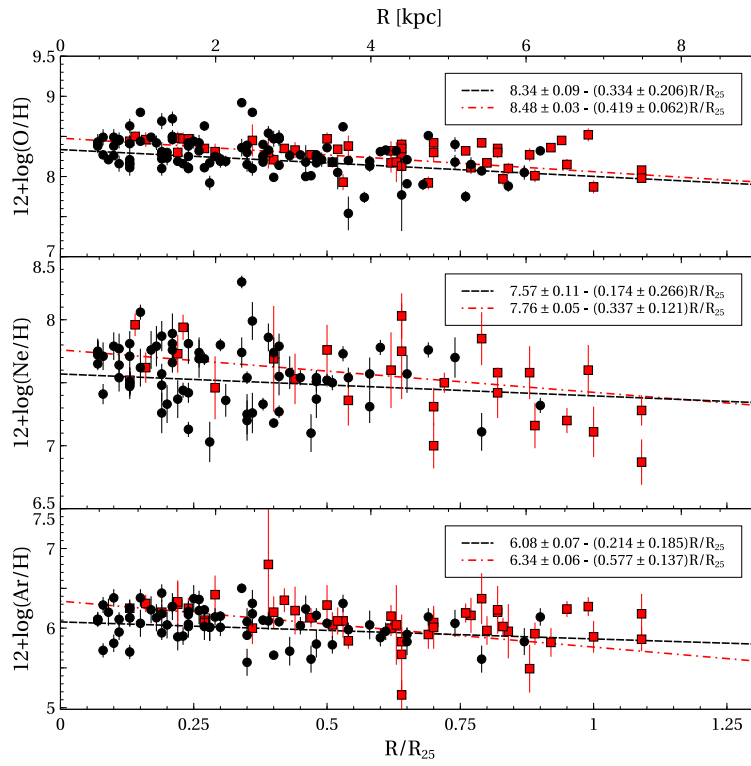


Fig. 3. Radial metallicity gradients in M33. Symbols are as in figure 1.

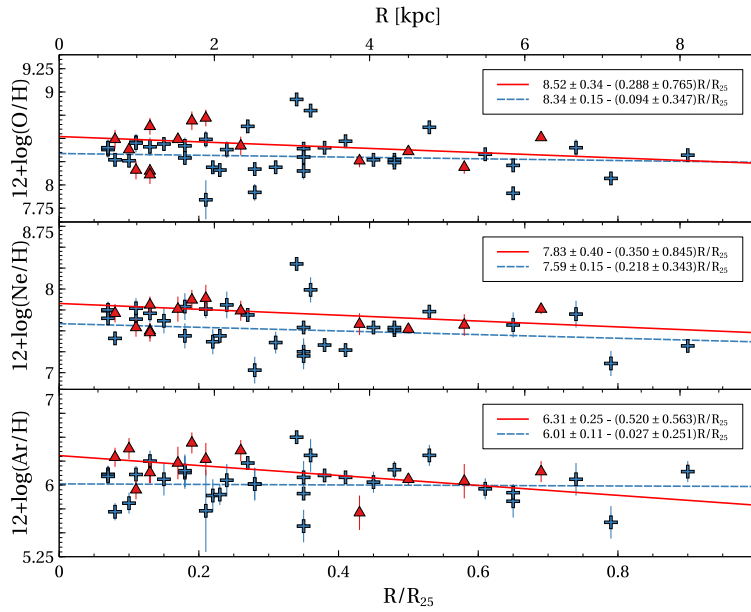


Fig. 4. Radial metallicity gradients from different Peimbert Types in M33. In red the data for Type I PNe are shown and in blue, the data for non-Type I PNe.

TABLE 2

LINEAR FITS FOR METALLICITY GRADIENTS IN M 31, THE MILKY WAY, M 33, AND NGC 300

	Oxygen				Neon				Argon			
	X_0	err	$\Delta X/\Delta R$ dex/kpc	err	X_0	err	$\Delta X/\Delta R$ dex/kpc	err	X_0	err	$\Delta X/\Delta R$ dex/kpc	err
M 31												
All PNe	8.46	0.03	-0.001	0.001	8.01	0.04	-0.002	0.001	6.22	0.05	-0.002	0.001
Type I	8.43	0.03	-0.002	0.001	8.03	0.05	-0.004	0.002	6.31	0.09	-0.005	0.002
non-Type I	8.57	0.03	-0.003	0.001	8.01	0.06	0.000	0.001	6.17	0.07	-0.000	0.001
H II reg.	8.76	0.10	-0.030	0.007	7.99	0.23	-0.036	0.016	6.38	0.18	-0.021	0.013
MW												
All PNe	8.85	0.05	-0.024	0.003	8.20	0.03	-0.021	0.005	6.58	0.03	-0.018	0.015
Type I	8.75	0.05	-0.019	0.002	8.24	0.06	-0.026	0.014	6.60	0.02	-0.010	0.006
non-Type I	8.84	0.05	-0.022	0.003	8.20	0.05	-0.027	0.009	6.45	0.03	-0.018	0.006
H II reg.	8.79	0.05	-0.040	0.005	8.21	0.04	-0.027	0.012	7.18	0.14	-0.071	0.029
M 33												
All PNe	8.34	0.07	-0.038	0.016	7.70	0.06	-0.036	0.030	6.17	0.06	-0.031	0.014
Type I	8.52	0.34	-0.032	0.020	7.83	0.40	-0.039	0.050	6.31	0.25	-0.058	0.030
non Type I	8.34	0.15	-0.010	0.020	7.59	0.15	-0.024	0.015	6.01	0.11	-0.010	0.020
H II reg.	8.48	0.03	-0.047	0.008	7.76	0.04	-0.043	0.010	6.34	0.04	-0.064	0.016
NGC 300												
PNe	8.37	0.03	-0.030	0.011	7.65	0.03	-0.029	0.013	6.31	0.02	-0.051	0.014
H II reg.	8.57	0.03	-0.077	0.008	7.71	0.05	-0.065	0.016	6.33	0.04	-0.104	0.017

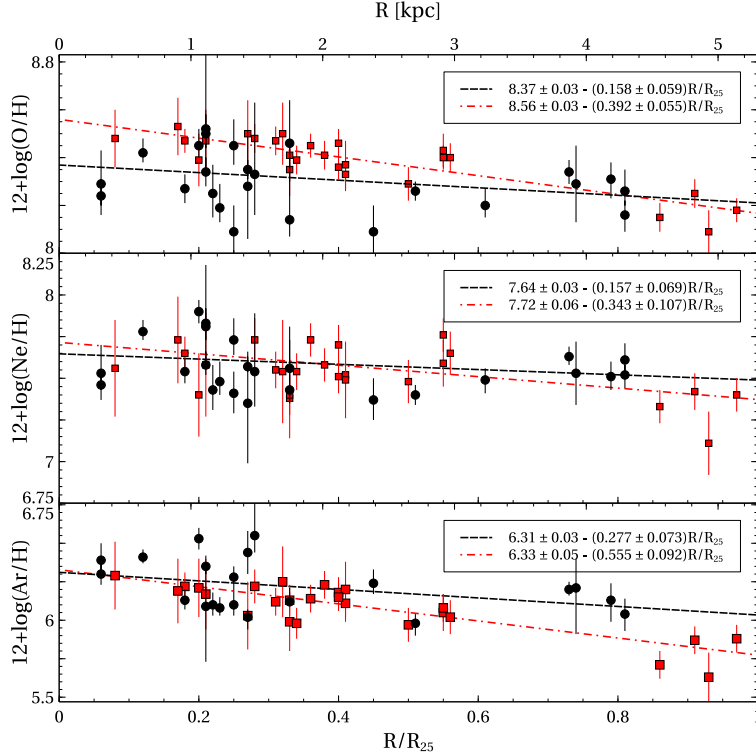


Fig. 5. Radial metallicity gradients in NGC 300. Symbols are as in figure 1.

metallicity and the stellar mass. However Ar abundance determinations have large uncertainties, therefore the results based on Ar only should be taken carefully.

When considering the PNe separated by Peimbert types, M31 shows a clear case where the gradients seem to be steepening with time since Type I PNe, which correspond to the youngest objects among the PN population, with ages lower than 1 Gyr, present steeper slopes than non-Type I PNe, with ages between 2 to 9 Gyr. Type I PN gradients are more similar to, but still much flatter than H II region slopes. The gradients for non-Type I PN are most probably altered by radial migration that have moved the old PNe from their initial galactocentric position in the galaxy. Type I PNe, due to their youth, have had less time to migrate from their place of birth, although the flatness of their gradients also indicate perturbations due to migration.

In the Milky Way, H II region and PNe gradients can be compared to the gradients of objects of similar ages as Cepheid stars (age younger than 0.1 Gyr) and Open Clusters (ages between 2 and more than 8 Gyr). H II regions and Cepheid stars present the same O/H gradients, which indicates that the chemical enrichment in the Galaxy has not increased in the last few hundreds of Myr. On the other hand PNe and Open Clusters (OC) present similar gradients, flatter than those of Cepheids and H II regions. This could indicate that the gradients steepen slowly with time (from -0.02 to -0.04 dex kpc^{-1} in several Gyr). Alternatively it could indicate that radial migration could have perturbed the slopes presented by these relatively old disk objects. Chemical evolution models for the Galaxy by Mollá et al. (2019) seem to favor the first option.

In the Milky Way a sort of step in the PN gradient seems to exist in the sense that inside $R \sim 14$ kpc, there is a measurable gradient of about -0.024 dex kpc^{-1} in the three elements. Outside this galactocentric distance, PNe show a flat slope. Stanghellini & Haywood (2018) reported the same phenomenon, based on the same data for PNe in the outskirts. However there are only a handful of objects detected in this zone, and a larger sample should be analyzed to confirm this step in abundances.

In general, the central abundances of O, Ne and Ar of PNe are similar to the central abundances of H II regions (the differences could be of about 0.2 dex), indicating that the central enrichment has not been important since the time of birth of PNe, and dust depletion of O in H II regions is not large. Although, due to the flat gradients of PNe, at galactocentric distance larger than about $0.5 R/R_{25}$, the average abundances in PNe are

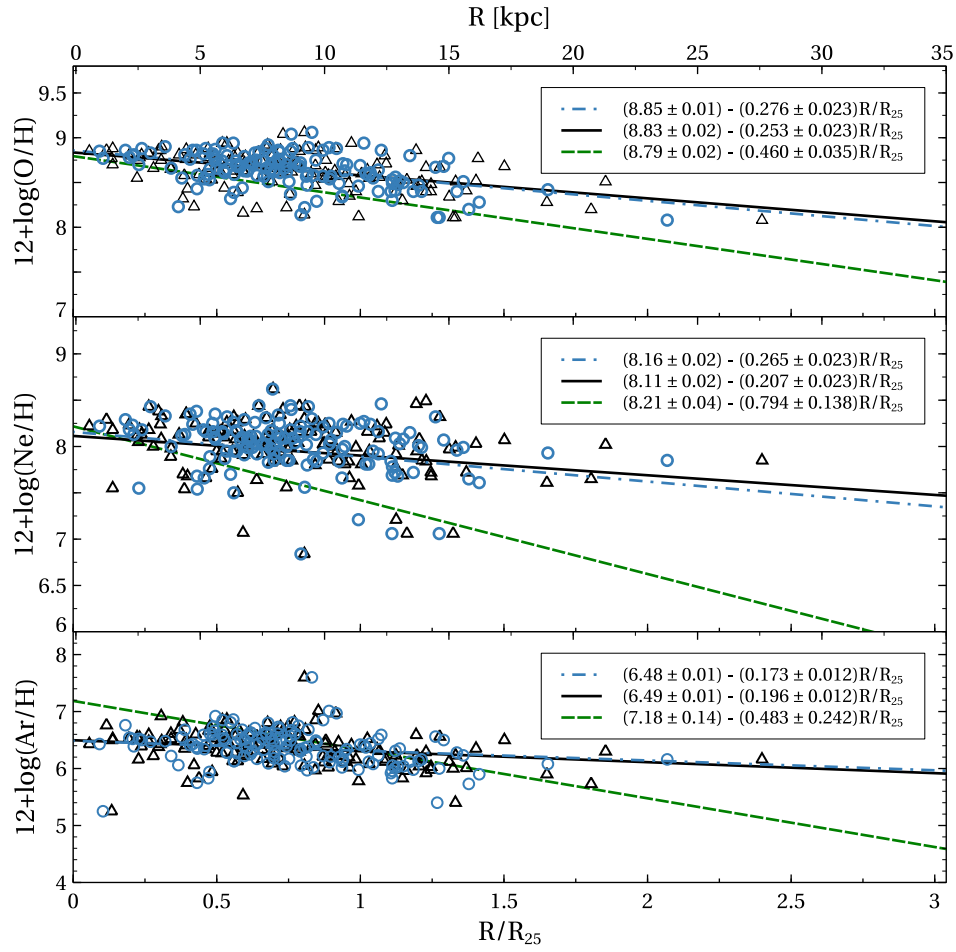


Fig. 6. Radial metallicity gradients of O, Ne and Ar, in the Milky Way, are presented. Open blue circles and black triangles are PNe with distances from Frew et al. (2016) and Stanghellini & Haywood (2010) respectively. Dotted-dashed line is the linear fit for F16 distances and the solid line is for Stanghellini & Haywood distances. Green dashed line is the linear fit for H II regions by Esteban et al. (2016).

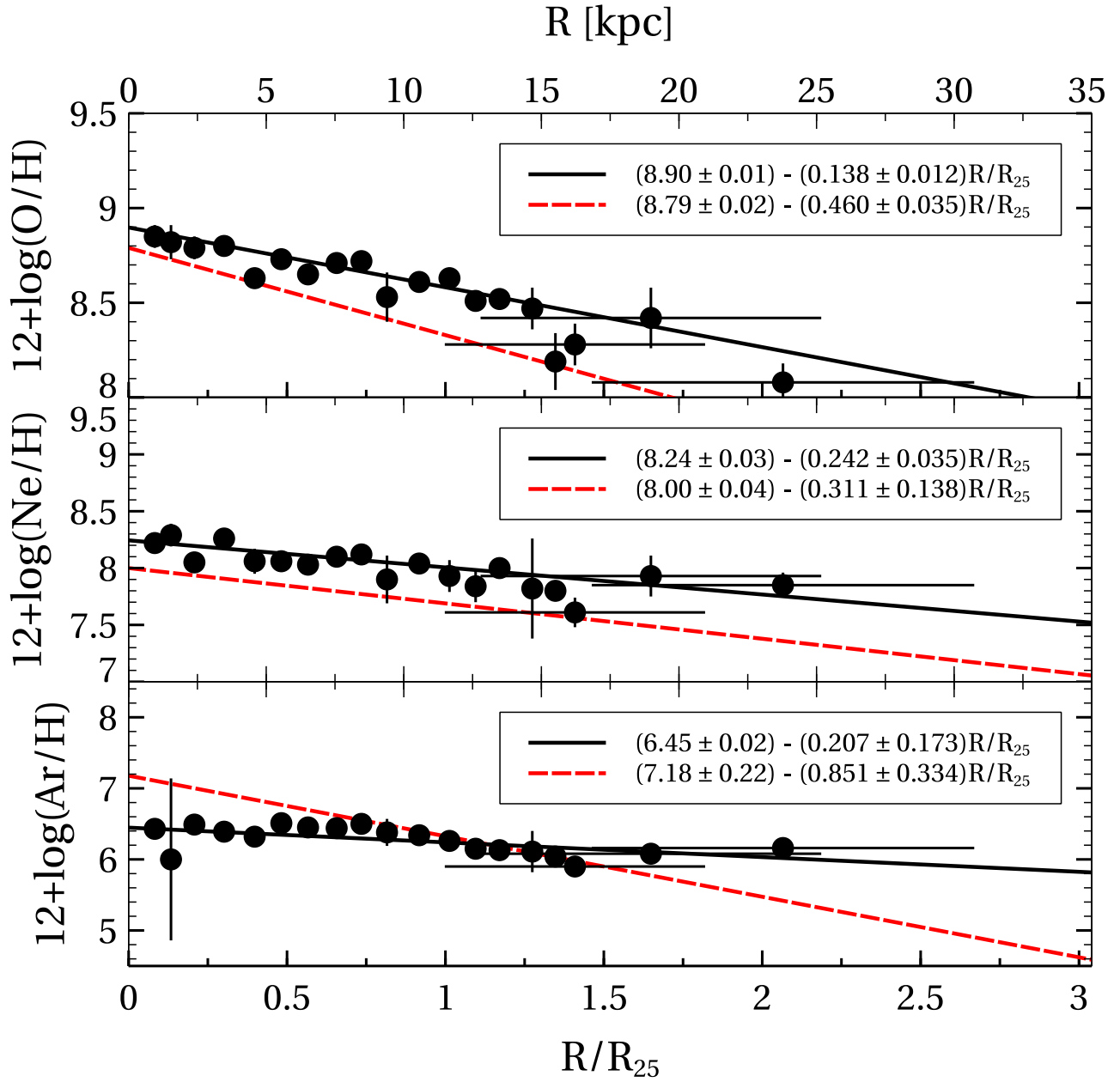


Fig. 7. Black circles correspond to PNe with F16 distances binned in bins of 1 kpc. Continuous lines are the fits for PNe and dashed lines are the fits for HII regions. On top we show the metallicity gradient for O, in the center the gradient for Ne, and at bottom the Ar metallicity gradient.

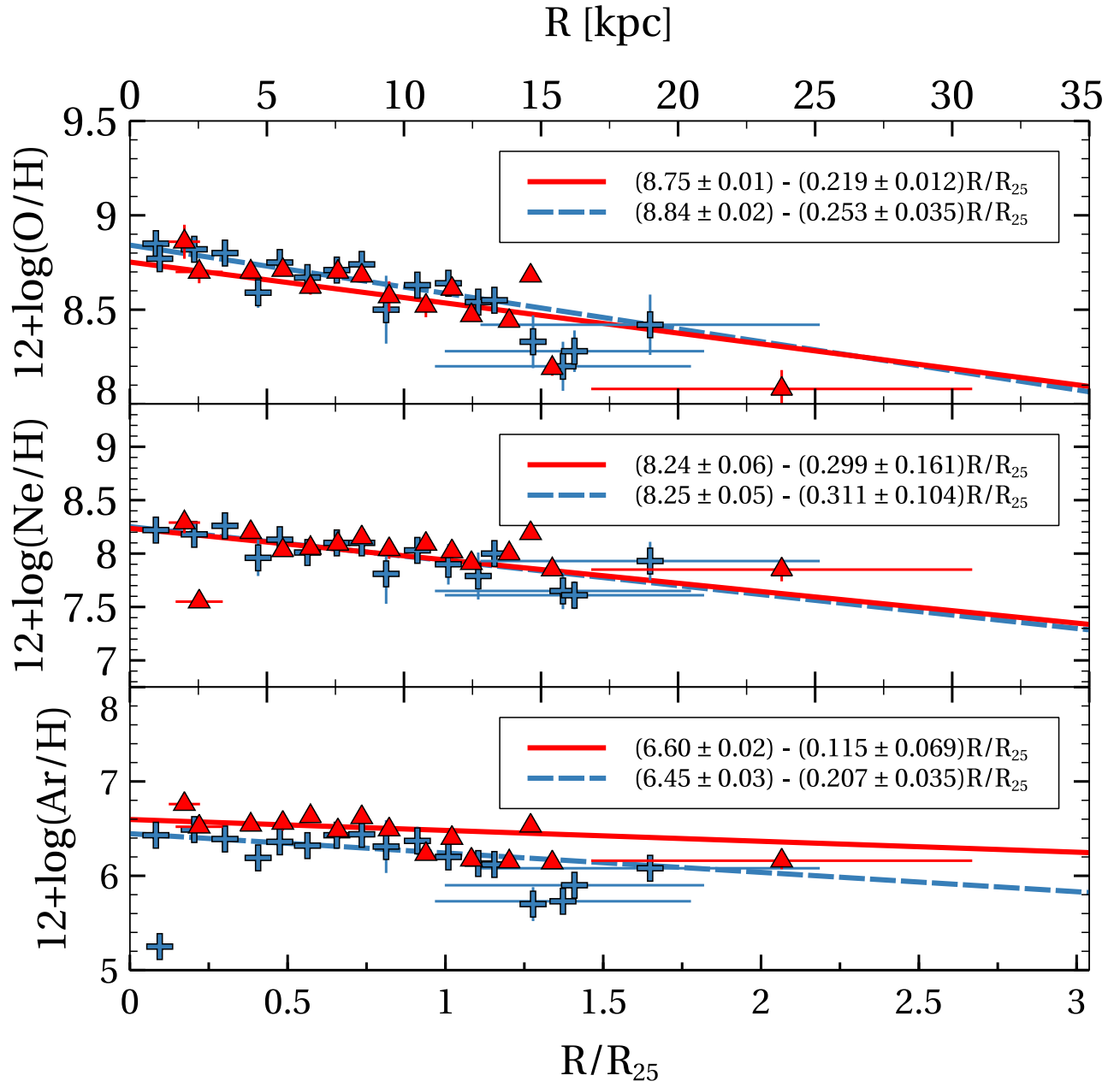


Fig. 8. The PNe of the MW with same binned distances as in figure 7. Red diamonds are Type I PNe and blue stars are non-Type I PNe. Continuous lines correspond to the linear fits for Type I's and the dotted lines correspond to fits for non-Type I's.

larger than the average abundances in H II regions.

It is found that in PNe formed in low metallicity environment ($Z \leq 0.004$, like in NGC 300), with initial masses of about $3 M_{\odot}$ or larger, the oxygen could have been modified by stellar nucleosynthesis and its value in the nebula does not represent the initial value at the time of stellar formation. This is not the case in larger metallicity environments or in stars with lower initial masses. In the former case we suggest to use Ar as an element showing the initial abundance in the nebula, in spite of Ar abundance determination has large uncertainties.

Our results are very useful for the computation of chemical evolution models in these galaxies, as the present ISM represented by H II regions and the older component represented by PNe can be used for constraining the models. Non-Type I PNe are very useful to analyze the effect of radial migration in disk galaxies.

Acknowledgements

This work received financial support from DGAPA-UNAM PAPIIT 103117 and CONACyT Project 241732. S.N.F.-D. acknowledges postdoctoral scholarship from project CONACyT 241732. We acknowledge an anonymous referee for her/his careful revision and comments that help to improve this manuscript.

REFERENCES

- Aller, L. H. 1942, *ApJ*, 95, 52
- Balick, B., Kwitter, K. B., Corradi, R. L. M., & Henry, R. B. C. 2013, *ApJ*, 774, 3
- Bresolin F., Gieren W., Kudritzki R-P., Pietrzyński G., Urbaneja M. A., & Carraro G. 2009, *ApJ*, 700, 309
- Bresolin F., Stasińska, G., Vílchez, J. M., Simon, J. D., & Rosolowsky, E. 2010, *MNRAS*, 404, 1679
- Cahn, J. H., Kaler, J. B., & Stanghellini, L. 1992, *A&AS*, 94, 399
- Carigi, L., & Peimbert, M. 2011, *RevMexAA*, 47, 139
- Ciardullo, R., Feldmeier, J. J., Jacoby, G. H., Kuzio de Naray, R., Laychak, M. B., & Durrell, P. R. 2002, *ApJ*, 577, 31
- Cioni, M.-R. L. 2009, *A&A*, 506, 1137
- Deharveng, L., Peña, M., Caplan, J., & Costero, R. 2000, *MNRAS*, 311, 329
- Delgado-Inglada, G., Morisset, C., & Stasińska, G. 2014, *MNRAS*, 440, 536
- Delgado-Inglada, G., Rodríguez, M., Peimbert, M., Stasińska, G., & Morisset, C. 2015, *MNRAS*, 449, 1797
- D’Odorico, S., Peimbert, M., & Sabbadin, F. 1976, *A&A*, 47, 341
- Draine, B. T., Aniano, G., Krause, O., et al. 2014, *ApJ*, 780, 172
- Esteban, C., Peimbert, M., García-Rojas, J., Ruiz, M. T., Peimbert, A., & Rodríguez, M. 2004, *MNRAS*, 355, 229
- Esteban, C., Carigi, L., Copetti, M. V. F., García-Rojas, J., Mesa-Delgado, A., Castañeda, H. O., & Péquignot, D. 2013, *MNRAS*, 433, 382
- Esteban, C., Mesa-Delgado, A., Morisset, C., & García-Rojas, J. 2016, *MNRAS*, 460, 4038
- Esteban, C., Fang, X., García-Rojas, J., & Toribio San Cipriano, L. 2017, *MNRAS*, 471, 987
- Fang, X., Zhang, Y., García-Benito, R., Liu, X.-W., & Yuan, H.-B. 2013, *ApJ*, 774, 138
- Fang, X., García-Benito, R., Guerrero, M. A., Liu, X., Yuan, H., Zhang, Y., & Zhang, B. 2015, *ApJ*, 815, 69
- Fernández-Martín, A., Pérez-Montero, E., Vílchez, J. M., & Mampaso, A. 2017, *A&A*, 597, A84
- Flores-Durán, S. N., Peña, M., & Ruiz, M. T. 2017, *A&A*, 601, A147
- Frew, D. J., Parker, Q. A., & Bojčić, I. S. 2016, *MNRAS*, 455, 1459 (F16)
- García-Rojas, J., Esteban, C., Peimbert, M., Rodríguez, M., Ruiz, M. T., & Peimbert, A. 2004, *ApJS*, 153, 501
- García-Rojas, J., Esteban, C., Peimbert, A., Peimbert, M., Rodríguez, M., & Ruiz, M. T. 2005, *MNRAS*, 362, 301
- García-Rojas, J., Esteban, C., Peimbert, M., Costado, M. T., Rodríguez, M., Peimbert, A. & Ruiz, M. T. 2006, *MNRAS*, 368, 253
- García-Rojas, J., Esteban, C., Peimbert, A., Rodríguez, M., Peimbert, M., & Ruiz, M. T. 2007, *RMxAA*, 43, 3
- Halle, A., Di Matteo, P., Haywood, M., & Combes, F. 2015, *A&A*, 578, A58
- Henry, R. B. C., Kwitter, K. B., & Balick, B. 2004, *AJ*, 127, 2284
- Henry, R. B. C., Kwitter, K. B., Jaskot, A. E., Balick, B., Morrison, A., & Milingo, J. B. 2010, *ApJ*, 724, 748
- Hernández-Martínez, L., Carigi, L., Peña, M., & Peimbert, M. 2011, *A&A*, 535, 118
- Karakas, A. I. 2010, *MNRAS*, 403, 1413
- Kingsburgh, R. L., & Barlow, M. J. 1994, *MNRAS*, 271, 257
- Kaler, J. B. 1980, *ApJ*, 239, 78
- Kimeswenger, S. & Barría, D. 2018, *A&A*, 616, L2
- Kwitter, K. B. & Henry, R. B. C. 2001, *ApJ*, 562, 804
- Kwitter, K. B., Lehman, E. M. M., Balick, B., & Henry, R. B. C. 2012, *ApJ*, 753, 12

- Maciel, W. J., Costa, R. D. D., & Ushida, M. M. M. 2003, *A&A*, 397, 667
- Martínez-Medina, L. A., Pichardo, B., Peimbert, A., & Carigi, L. 2017, *MNRAS*, 468
- McConnachie, A. W., Irwin, M. J., Ferguson, A. M. N., et al. 2005, *MNRAS*, 356, 979
- McConnachie, A. W., Irwin, M. J., Ibata, R. A., et al. 2009, *Nature*, 461, 66
- Magrini L., Stanghellini, L., & Villaver, E. 2009, *ApJ*, 696, 729
- Magrini L., Corbelli, E. & Galli, D. 2007, *A&A*, 470, 843
- Magrini L., Stanghellini, L., Corbelli, E., Galli, D., & Villaver, E. 2010, *A&A*, 512, A63
- Magrini L., Coccato, L., Stanghellini, L., Casasola, V., & Galli, D. 2016, *A&A*, 588, A91
- Milingo, J. B., Kwitter, K. B., Henry, R. B. C., & Souza, S. P. 2010, *ApJ*, 711, 619
- Mollá, M., Díaz, Á. L., Cavichia, O., Gibson, B. K., Maciel, W. J., Costa, R. D. D., Ascasibar, Y., & Few, C. G. 2019, *MNRAS*, 482, 3071
- Peimbert, M. 1978, in *Planetary Nebulae*, IAU Symp. 76, Dordrecht:Reidel, , p. 224
- Peña, M., Reyes-Pérez, J., Hernández-Martínez, L., & Pérez-Guillén, M. 2012, *A&A*, 547, 78
- Peña, M., Stasińska, G., & Richer, M. G. 2007, *A&A*, 476, 745
- Rodríguez, M. & Delgado-Inglada, G. 2011, *ApJL*, 733, 50
- Ruiz-Lara, T., Few, C. G., Florido, E., Gibson, B. K., Pérez, I., & Sánchez-Blázquez, P. 2017, *A&A*, 608, 126
- Sanders, N. E., Caldwell, N., McDowell, J., & Harding, P. 2012, *ApJ*, 758, 133
- Sánchez-Menguiano L., Sánchez S. F., Pérez I., Ruiz-Lara T., Galbany L., Anderson J. P., Krühler T., Kuncarayakti H., & Lyman J. D. 2018, *A&A*, 609, A119
- Sánchez, S. F., Rosales-Ortega, F. F., Iglesias-Páramo, J., Mollá, M., Barrera-Ballesteros, J., et al. 2014, *A&A*, 563, A49
- Searle, L.. 1971, *ApJ*, 168, 327
- Stanghellini, L. & Haywood, M. 2010, *ApJ*, 714, 1096 (S10)
- Stanghellini, L. & Haywood, M. 2018, *ApJ*, 862, 45
- Stanghellini, L., Shaw, R. A., & Villaver, E. 2008, *ApJ*, 689, 194
- Stasińska G., Peña M., Bresolin F., & Tsamis Y. G. 2013, *A&A*, 552, 12
- Ventura, P., Stanghellini, L., Di Criscienzo, M., García-Hernández, D. A., & Dell' Agli, F. 2016, *MNRAS*, 460, 3940
- Zaritsky, D., Kennicutt, R. C., Jr, & Huchra J. P. 1994, *ApJ*, 420, 87
- Zurita, A., & Bresolin, F. 2012, *MNRAS*, 427, 1463

S. N. Flores-Durán: Instituto de Astronomía, Universidad Nacional Autónoma de México, Apdo. Postal 70264, Ciudad de México, 04510, México).

M. Peña: Instituto de Astronomía, Universidad Nacional Autónoma de México, Apdo. Postal 70264, Ciudad de México, 04510, México (miriam@astro.unam.mx).